

***Ab initio* study of charge order in Fe₃O₄**Z. Szotek,¹ W. M. Temmerman,¹ A. Svane,² L. Petit,² G. M. Stocks,³ and H. Winter⁴¹*Daresbury Laboratory, Daresbury, Warrington, WA4 4AD Cheshire, United Kingdom*²*Institute of Physics and Astronomy, University of Aarhus, DK-8000 Aarhus C, Denmark*³*Metals and Ceramics Division, Oak Ridge National Laboratory, Oak Ridge, Tennessee 37831-6114, USA*⁴*INFP, Forschungszentrum Karlsruhe GmbH, Postfach 3640, D-76021 Karlsruhe, Germany*

(Received 12 February 2003; revised manuscript received 15 May 2003; published 19 August 2003)

We present a self-interaction corrected local spin-density study of the electronic structure and possible charge order of magnetite Fe₃O₄. The issue of charge order in magnetite is explored in both cubic and orthorhombic structures, the latter being an approximation to the true, low-temperature, monoclinic structure. We find that the Verwey charge ordered phase is not the ground-state solution for this compound either in cubic or orthorhombic structure. We conclude that the structural distortions, more than localization/delocalization correlations, are responsible for the charge disproportionation in the low-temperature phase.

DOI: 10.1103/PhysRevB.68.054415

PACS number(s): 75.10.Lp, 75.50.Bb

I. INTRODUCTION

Based upon its high magnetoresistive properties, magnetite Fe₃O₄ is a system of interest for such technological applications as computer memory, magnetic recording, and other “spintronic” devices. It has been extensively studied for the past 60 years,¹ but despite such an extended effort the issue of a possible charge order below the so-called Verwey transition temperature, $T_V = 122$ K, has not been understood yet.² Above the Verwey transition temperature, magnetite is thought to be a half metal with a highest known T_C of 860 K. At the transition temperature, the conductivity of the system decreases abruptly by two orders of magnitude, as a small gap opens up in the density of states spectrum.³ This first-order metal-insulator transition⁴ is associated with a lattice distortion from cubic to monoclinic, which however has not been fully resolved.⁵⁻⁷ The transition has been viewed as an order-disorder transition in relation to the arrangement of cations on the octahedral sites of the inverse spinel structure whose formal chemical formula can be written as $\text{Fe}_A^{3+} [\text{Fe}^{2+}, \text{Fe}^{3+}]_B \text{O}_4^{2-}$, where A and B refer to the interstitial, i.e., tetrahedral and octahedral sites, respectively. This simple ionic picture implies that magnetite is a mixed-valent compound. The A sublattice is occupied only by Fe^{3+} cations in a ferromagnetic arrangement, while the B sublattice is occupied by both Fe^{2+} ($B1$ -site) and Fe^{3+} ($B2$ -site) cations, also in a ferromagnetic manner which, however, is antiferromagnetically aligned to the ferromagnetic order on the A sublattice. The oxygen atoms occupy the face-centered-cubic (fcc) close-packed sites. The Fe^{2+} cation can be viewed as Fe^{3+} plus an “extra” electron, hopping freely between the octahedral sites above the Verwey transition, while below the transition these extra electrons become localized or quasilocated and some kind of long-range order sets in on the B sublattice. Verwey, who argued that below the transition temperature T_V , the Fe^{3+} and Fe^{2+} cations order in alternate (001) planes, looked upon this transition as an electron localization-delocalization transition. The Mössbauer spectra clearly demonstrate the existence of two types of localized ions on the octahedral sites.⁸ The low-temperature structure

is a rhombohedral distortion of the cubic spinel arrangement to the first approximation,⁹ but this splits in the ratio 3:1 for the occurrence of the Fe^{2+} and Fe^{3+} cations on the corner-sharing tetrahedra that are formed by the octahedral sites. This is not consistent with the Anderson condition of minimum electrostatic repulsion, implying the ratio of 2:2.¹⁰ A recent combined high-resolution x-ray and neutron powder-diffraction study⁷ confirmed a small charge disproportionation of about 0.2 electron on the octahedral sites, and a violation of the Anderson condition. The current experimental situation suggests that the long-range order present below the Verwey transition is much more complicated than the charge order first proposed by Verwey. Some experiments claim that there exists no charge order on the octahedral sites.^{11,12}

In this paper, we present an application of the self-interaction corrected local spin-density (SIC-LSD) approximation to Fe₃O₄. The SIC-LSD method allows the *ab initio* realization of valencies through total-energy calculations for configurations of Fe^{2+} and Fe^{3+} cations. The method includes all band-structure effects of the delocalized Fe and O electrons, including their hybridization, as well as the electronic structure of the localized Fe electrons. As such this methodology has been able to describe the valencies of the rare earths successfully.¹³ Here, we concentrate on the total energies for different d -electron configurations on the octahedral sites, defining Fe valencies, and try to establish whether the simple charge order postulated by Verwey is the ground-state solution. Apart from the Verwey order we also consider other obvious arrangements of Fe valencies on the octahedral sites. There have been other first-principles studies of magnetite,¹⁴⁻¹⁶ however, here different Fe valencies and charge order scenarios have been studied by an *ab initio* method. In Refs. 15 and 16, the (local-density approximation) LDA+U method has been used to study the Verwey insulating phase albeit in the cubic structure only, and neither the total energies nor other charge order phases have been considered. In Ref. 16, in addition, the optical properties of magnetite have been studied.

The remainder of the paper is organized as follows. In the following section, we briefly present the theoretical back-

ground of the SIC-LSD approach. In Sec. III, the technical and computational details regarding the application to magnetite are elaborated upon. In Sec. IV, we present total-energy and density of states calculations. We also study the charge order and different Fe valencies on the octahedral sites, and try to establish the ground-state configuration. The paper is concluded in Sec. V.

II. THEORY

The basis of the SIC-LSD formalism is a self-interaction free total-energy functional E^{SIC} , obtained by subtracting from the LSD total-energy functional E^{LSD} a spurious self-interaction of each occupied electron state ψ_α ,¹⁷ namely,

$$E^{SIC} = E^{LSD} - \sum_{\alpha}^{occ} \delta_{\alpha}^{SIC}. \quad (1)$$

Here α numbers the occupied states and the self-interaction correction for the state α is

$$\delta_{\alpha}^{SIC} = U[n_{\alpha}] + E_{xc}^{LSD}[\bar{n}_{\alpha}], \quad (2)$$

with $U[n_{\alpha}]$ being the Hartree energy and $E_{xc}^{LSD}[\bar{n}_{\alpha}]$ the LSD exchange-correlation energy for the corresponding charge density n_{α} and spin density \bar{n}_{α} .

The SIC-LSD approach can be viewed as an extension of LSD in the sense that the self-interaction correction is only finite for spatially localized states, while for Bloch-like single-particle states E^{SIC} is equal to E^{LSD} . Thus, the LSD minimum is also a local minimum of E^{SIC} . A question now arises, whether there exist other competitive minima, corresponding to a finite number of localized states, which could benefit from the self-interaction term without losing too much of the energy associated with band formation. This is often the case for rather well localized electrons such as the $3d$ electrons in transition-metal oxides or the $4f$ electrons in rare-earth compounds. It follows from minimization of Eq. (1) that within the SIC-LSD approach such localized electrons move in a different potential than the delocalized valence electrons which respond to the effective LSD potential. For example, in the case of magnetite, five (Fe^{3+}) or six (Fe^{2+}) Fe d electrons move in the SIC potential, while all other electrons feel only the effective LSD potential. Thus, by including an explicit energy contribution for an electron to localize, the *ab initio* SIC-LSD describes both localized and delocalized electrons on an equal footing, leading to a greatly improved description of static Coulomb correlation effects over the LSD approximation.

In order to make the connection between valency and localization more explicit, it is useful to define the nominal valency as

$$N_{val} = Z - N_{core} - N_{SIC},$$

where Z is the atomic number (26 for Fe), N_{core} is the number of core (and semicore) electrons (18 for Fe), and N_{SIC} is the number of localized, i.e., self-interaction corrected, states (either five or six, respectively, for Fe^{3+} and Fe^{2+}). Thus, in this formulation the valency is equal to the integer number of

electrons available for band formation. To find the valency we assume various atomic configurations, consisting of different numbers of localized states, and minimize the SIC-LSD energy functional of Eq. (1) with respect to the number of localized electrons. The SIC-LSD formalism is governed by the energetics due to the fact that for each orbital the self-interaction correction differentiates between the energy gain due to hybridization of the orbital with the valence bands and the energy gain upon localization of the orbital. Whichever wins determines if the orbital is part of the valence band or not and in this manner also leads to the evaluation of the valency of elements involved. The self interaction correction depends on the choice of orbitals and its value can differ substantially as a result of this. Therefore, one has to be guided by the energetics in defining the most optimally localized orbitals to determine the absolute energy minimum of the SIC-LSD energy functional. The advantage of the SIC-LSD formalism is that for such systems as transition-metal oxides or rare-earth compounds the lowest-energy solution will describe the situation where some single-electron states may not be Bloch-like. For magnetite, these would be the Fe $3d$ states, but not the O $2p$ states, as trying to localize the latter is energetically unfavorable.

In the present work, the SIC-LSD approach has been implemented¹⁸ within the linear muffin-tin-orbital atomic sphere approximation (ASA) band-structure method,¹⁹ in the tight-binding representation.²⁰ The electron wave functions are expanded in terms of the screened muffin-tin orbitals, and the minimization of E^{SIC} becomes nonlinear in the expansion coefficients.

III. CALCULATIONAL DETAILS

As mentioned earlier, magnetite crystallizes in the fcc inverse spinel structure with two formula units (14 atoms) in the primitive unit cell, and the space group is $Fd\bar{3}m$. In the actual calculations, an additional 16 empty spheres have been used in order to obtain better space filling and to minimize the ASA overlap. Concerning the linear muffin-tin basis functions, we have used $4s$, $4p$, and $3d$ partial waves on all Fe atoms, and treated them as low waves.²¹ Including also $4f$ basis functions on the Fe sites, treated as intermediate waves, is of no substantial importance for the final results. On the oxygens only $2s$ and $2p$ partial waves have been treated as low waves, while the $3d$ waves have been treated as intermediate. On the empty spheres the $1s$ waves have been considered as low waves and the $2p$'s as intermediate waves. The empty spheres are necessary to obtain half-metallic solution with the LSD, whose self-consistent charge densities have been used to start SIC-LSD calculations.

Although, below the Verwey transition, the cubic structure undergoes a monoclinic distortion, we have first explored the charge ordered phases on the basis of the cubic structure and then extended the study to the distorted structure. Since the true monoclinic structure has not been fully resolved, our calculations for the low-temperature phase have been performed for two orthorhombic structures, given in Refs. 5 and 7, as closest approximations to the monoclinic structure. In the latter work, the refined atom positions were obtained us-

ing a combination of high-resolution x-ray and neutron powder diffraction. The respective space groups used are $Pmc2_1$ and $P2/c$, each with 56 atoms in the unit cell. However, for reliable calculations empty spheres have been included, increasing the total number of sites to 104 in the first case, and 120 for the refined structure of Wright *et al.*⁷

To make the SIC-LSD calculations feasible, for the orthorhombic setups we had to restrict to minimum basis sets, in particular, $4s, 4p, 3d$ low waves have been used on every Fe atom, $2s, 2p$ low waves and intermediate $3d$ waves on all oxygen atoms and only $1s$ low waves and intermediate $2p$ waves on the empty spheres. Also, the number of k points in the irreducible Brillouin zone had to be reduced to 18 k points.

To study charge order, we have implemented three obvious scenarios. First, we have considered the simple Verwey charge order, where it is assumed that the tetrahedral sites are occupied by Fe³⁺ ions, while on all the octahedral sites Fe alternates between Fe³⁺ (five d electrons move in the SIC-LSD potential) and Fe²⁺ (six d electrons move in the SIC-LSD potential) in the successive (001) planes. Subsequently, we refer to this as the Verwey charge order scenario. In the second scenario, we assume that all tetrahedral and octahedral sites are trivalent, namely Fe³⁺. Finally, in the third scenario we assume all the tetrahedral sites to be Fe³⁺, and all the octahedral sites to be Fe²⁺. In what follows, we shall refer to these calculations as scenarios 1–3, respectively.

Note that for a divalent Fe atom one needs to consider six d electrons moving in the SIC potential. Five of the electrons fill up the full manifold of one spin component, while the sixth electron has the freedom to populate either of the five states of the other spin component (three t_{2g} and two e_g states in the cubic symmetry). As a result, five separate self-consistent total-energy calculations have to be performed, for all different structures and scenarios involving divalent Fe's, to find the lowest-energy solution. In what follows, only the results of the lowest-energy solutions are presented and discussed.

IV. RESULTS AND DISCUSSION

A. Densities of states

In Fig. 1, we compare for the cubic structure the LSD total and species-decomposed densities of states (DOS) with the SIC-LSD counterparts where the Verwey charge order has been implemented. In this figure, both spin components are displayed. In Fig. 2, we compare separately the LSD spin-decomposed DOS for the tetrahedral and octahedral sites with the respective DOS from the SIC-LSD calculations, where the octahedral sites are additionally split into Fe³⁺ and Fe²⁺. The first thing to note about Fig. 1 is that the LSD calculations find half-metallic DOS, while a small band gap opens up in both spin channels of the SIC-LSD densities of states, as a result of the Verwey charge order implemented on the octahedral sites. The gap is about 0.35 eV, which is more than two times the experimental gap found in photoemission for magnetite below the Verwey transition temperature, but in good agreement with the LDA+U calculation of Anisimov *et al.*,¹⁵ although the SIC-LSD gap has the p - d

charge-transfer character, while the LDA+U gap occurs between d states of the octahedral Fe ions. Note that due to opening of the SIC-LSD gap, the unoccupied Fe $3d$ states have been shifted up in energy, away from the Fermi level, while the occupied Fe $3d$ states appear well below the valence band, which is composed mostly of oxygen $2p$ with a small admixture of Fe d states. In the LSD plots, the spin-up Fe $3d$ states occur at the Fermi level, while there is a well defined gap in the other spin component. In addition, the predominantly oxygenlike valence band is much more structured in the case of LSD, due to strong hybridization with Fe $3d$ states, which appear at the top of the valence band. Looking at all different types of Fe sites in both the calculations (see Fig. 2), it is clear that the Fe- A sites in the SIC-LSD calculations do not contribute to DOS at the Fermi level, so there is a well defined gap in both spin channels for these sites. The A sites in the LSD calculation exhibit a very small density of states in the spin-up component, and a gap in the other spin channel. The octahedral B sites in the LSD calculations exhibit a gap in one spin component and in the other spin component well hybridized states can be observed at the Fermi level, giving rise to the half-metallic ground state. Among the octahedral sites in the SIC-LSD calculations, the B sites occupied by Fe³⁺ ions show similar DOS to the LSD calculations for the octahedral ions, except for the gap appearing in the SIC-LSD case in both spin channels, and the localized spin-down Fe³⁺ states occurring well below the valence bands. Regarding the unoccupied Fe $3d$ states, the spin-up states for the Fe²⁺ sites lie higher in energy than the corresponding states for the Fe³⁺ sites. The small peak observed just below the valence band is due to the sixth localized $3d$ state, while the remaining five localized d states are visible at about 8.0 eV in the other spin component.

In Fig. 3, we show the total and partial Fe and O densities of states for the second SIC-LSD scenario, namely, for the case where all Fe sites, tetrahedral and octahedral alike, are 3+. The DOS are half metallic, with a gap in one spin component and hybridized Fe-O states occurring at the Fermi level in the other spin component. The DOS of localized Fe $3d$ states appear well below the valence band at about 13.0 eV. Note substantial differences of these DOS with respect to the LSD result of Fig. 1. The reason being that in the LSD all electrons move in the effective LSD potential, while in the 3+ scenario, the Fe $3d$ electrons respond to the SIC potential. Due to this localizing potential the total weight of the occupied $3d$ states is shifted well below the valence band, while in the LSD picture they appear at the top of the valence band, strongly hybridizing with the O $2p$ states. From the A -Fe and B -Fe site decomposed spin-polarized DOS in Fig. 4 we can see that the tetrahedral sites do not contribute at the Fermi level. The half-metallic behavior is entirely due to the hybridization of the unoccupied $3d$ states of the octahedral Fe sites with the oxygen $2p$ states.

Finally, the LSD and SIC-LSD densities of states for the orthorhombic structures (not displayed in this work) show similar features to their counterparts in the cubic structure, when the respective tetrahedral and octahedral ions are compared. Specifically, a small energy gap of about 0.1 eV and insulating solutions are observed in the charge ordered state

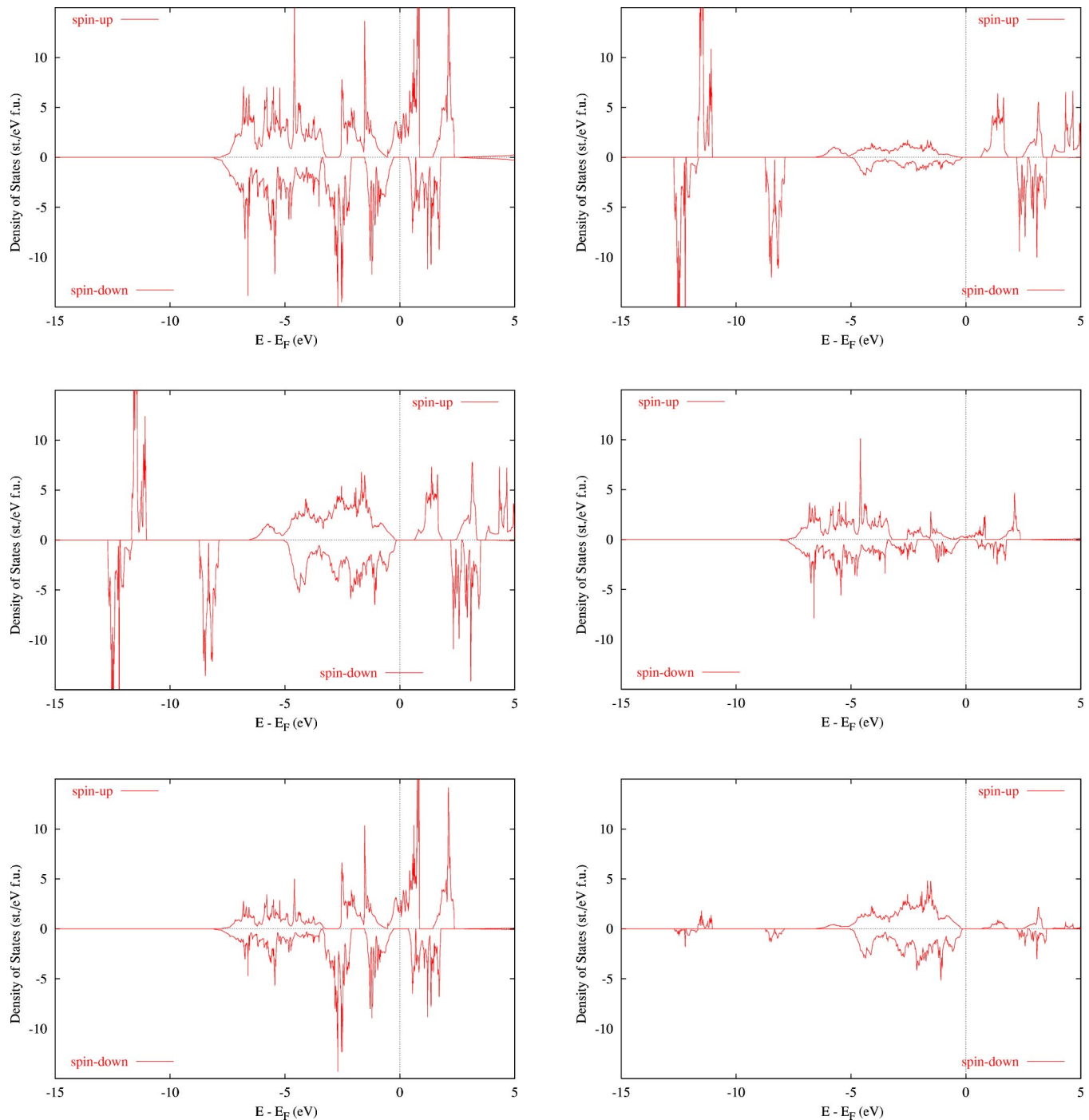


FIG. 1. (Color online) Spin-polarized total (top row), Fe (middle row) and O (bottom row) partial densities of states from the LSD calculation (left column) in comparison with the SIC-LSD (right column) counterparts for the Verwey charge ordered phase in the inverse spinel structure. The partial DOS for empty spheres are of no significance and therefore have not been shown.

for both orthorhombic symmetries. Note that in both orthorhombic structures that were studied, there are six crystallographically different B sites which are subsequently referred to as $B1, \dots, B6$.⁵ Nevertheless, we still have only two types of Fe ions, divalent and trivalent. Concerning the tetrahedral (A) sites, there are four different crystallographic positions in the structure with $Pmc2_1$ symmetry, but only two A -type positions in the structure with $P2/c$ symmetry.

Detailed comparison of the densities of states for all different crystallographic structures that we have implemented here reveals that the second scenario in the orthorhombic structure with the $Pmc2_1$ symmetry leads to metallic rather than half-metallic DOS. This result is caused by the fact that the Fermi level moves slightly into the Fe- A $3d$ peak, which is unoccupied in the cubic structure. However, for the refined orthorhombic structure of Ref. 7, with $P2/c$ symmetry, we

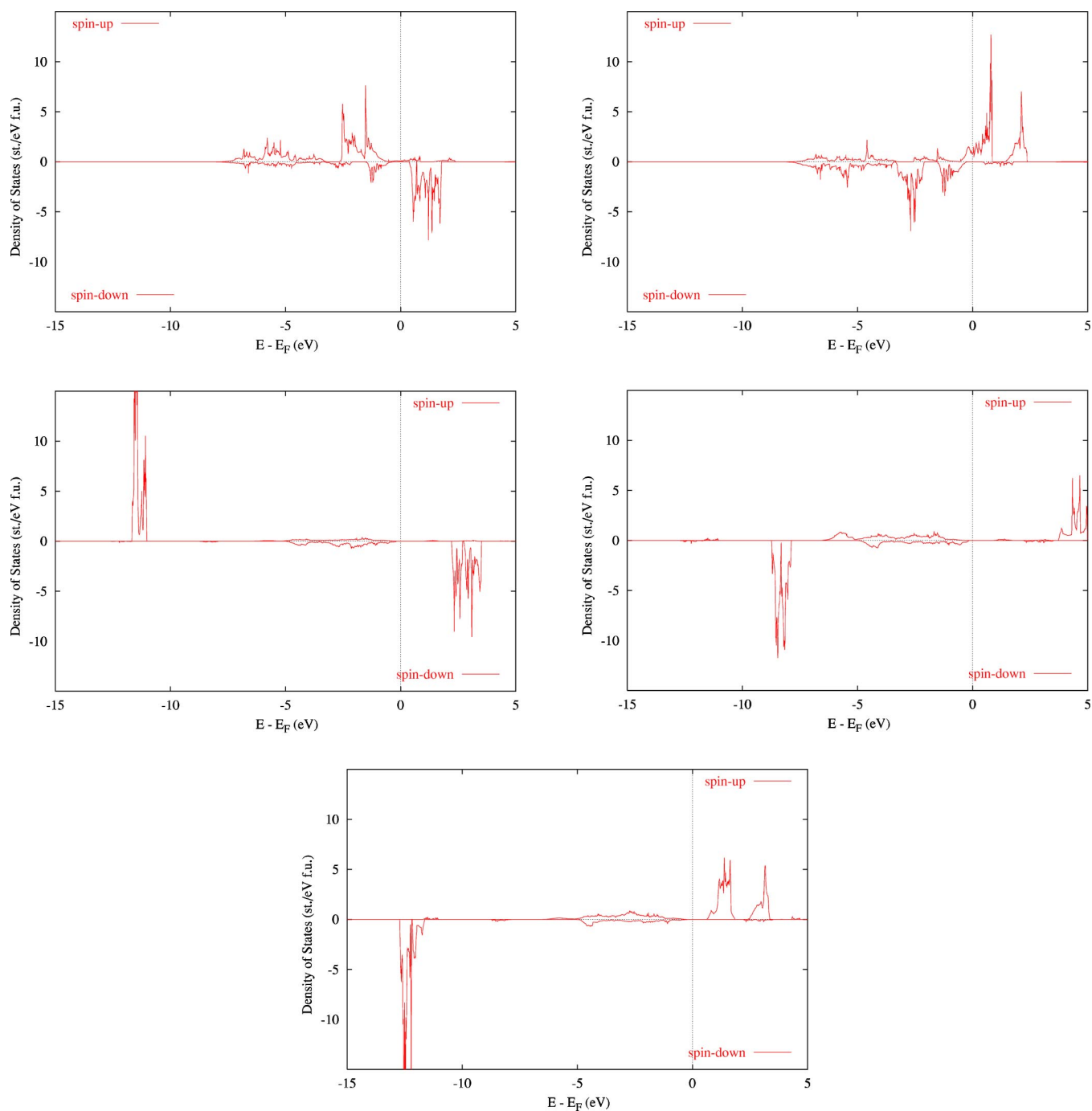


FIG. 2. (Color online) Spin-polarized densities of states for the A (top row) and B1 (middle row) Fe sites in the LSD calculation (left column) [note that in the LSD there is only one type of octahedral sites ($B1 \equiv B2 \equiv B$)] in comparison to the respective A (top row), B1 (middle row), and B2 (bottom row) Fe sites from the SIC-LSD calculation (right column) in the Verwey charge ordered phase.

again recover a half-metallic solution for the all trivalent configurations. As in the cubic structure, the Fe-A 3d peak is fully unoccupied. This appears to indicate a great sensitivity of the half-metallic solution to atom positions in the low-temperature structure.

B. Total energies and charge order

In this section, we concentrate on the total energies, spin magnetic moments, and charge disproportionation on octahe-

dral sites, obtained for the scenarios studied here. Tables I and II summarize for the cubic and orthorhombic structures, respectively, the spin magnetic moments on Fe sites and energy differences with respect to the ground-state configuration of the most favorable scenario.

Comparing total energies for the LSD and three different SIC-LSD charge order scenarios in either cubic (Table I) or orthorhombic (Table II) structure, one can see that the second scenario, with all Fe's in the trivalent configuration, is the lowest-energy solution. It is followed by the Verwey charge

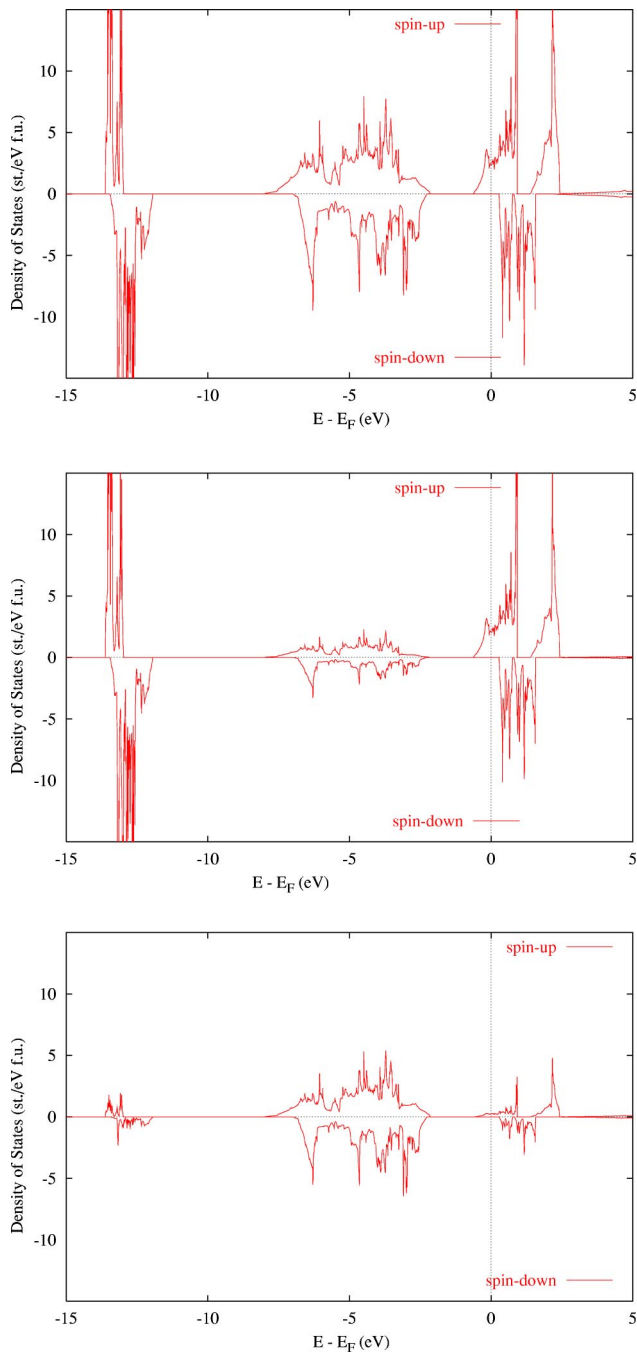


FIG. 3. (Color online) Spin-polarized total (top), Fe (middle), and O partial (bottom) densities of states for the second charge order scenario, namely, with trivalent configuration on all Fe sites in the SIC-LSD implementation.

order scenario, then the third scenario, and finally the LSD, which is the most unfavorable result. The significant energy difference of 113 mRy per formula unit (Table I), found between the scenario SIC(1) and scenario SIC(2), renders the simple Verwey ordering highly unlikely as an explanation for the properties in the low-temperature phase of magnetite. The last two columns of Table I, ΔE_{BF} and ΔE_{SIC} , representing, respectively, the loss in band formation/hybridization energy and gain in localization energy, relative

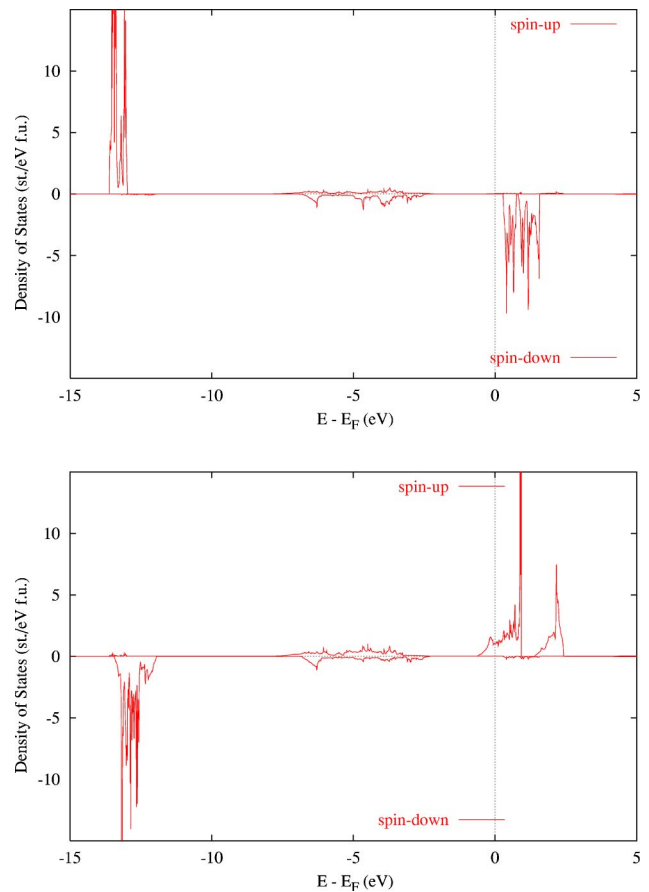


FIG. 4. (Color online) Spin-polarized densities of states for the A- (top) and B1- (bottom) Fe sites for the second scenario, namely, with trivalent configuration on all, tetrahedral and octahedral, Fe sites in the SIC-LSD implementation. Note that in this scenario there is only one type of octahedral sites ($B1 \equiv B2 \equiv B$).

to the respective values of the ground-state configuration, provide further physical understanding of this finding. While the localization energy favors more localized states, and hence the formation of Fe^{2+} on the B2 octahedral sites, the

TABLE I. Total and type-decomposed spin magnetic moments (in Bohr magnetons μ_B) for LSD and three different SIC-LSD scenarios for the cubic structure. Concerning types, only different Fe types are listed. Note that in the LSD, SIC(2), and SIC(3) calculations there is only one type of octahedral sites ($B1 \equiv B2 \equiv B$). Also given are the total-energy differences (in mRy/formula unit) with respect to the ground-state configuration. These energy differences are further decomposed into the energy loss in band formation/hybridization (ΔE_{BF}) and the energy gain due to localization (ΔE_{SIC}), both relatively to the respective energies of the ground-state configuration, which is the all Fe^{3+} scenario.

Scenario	M_{total}	M_{Fe_A}	$M_{\text{Fe}_{B1}}$	$M_{\text{Fe}_{B2}}$	ΔE	ΔE_{BF}	ΔE_{SIC}
LSD	4.00	3.40	-3.57	-3.57	894	-118	1012
SIC(1)	4.00	4.00	-3.57	-4.08	113	168	-55
SIC(2)	4.00	4.02	-3.90	-3.90	0	0	0
SIC(3)	2.00	4.01	-3.47	-3.47	374	475	-101

TABLE II. Total and type-decomposed spin magnetic moments (in Bohr magnetons μ_B) for LSD and three different SIC-LSD scenarios for the orthorhombic structures. Concerning types, only different Fe types are listed. In the LSD column for the $P2/c$ symmetry, 4.00(–) means that the magnetic moment is a tiny fraction less, but within better than 0.5% equal to $4.00\mu_B$. Also given are the total-energy differences (in mRy/formula unit) with respect to the ground-state configuration.

	LSD	SIC(1)	SIC(2)	SIC (3)
<i>Pmc2₁</i> symmetry				
M_{total}	4.00	4.00	4.02	2.00
M_{FeA1}	3.39	4.13	4.14	4.14
M_{FeA2}	3.32	4.13	4.13	4.15
M_{FeA3}	3.30	4.14	4.16	4.17
M_{FeA4}	3.34	4.15	4.16	4.16
M_{FeB1}	–3.40	–3.58	–3.88	–3.50
M_{FeB2}	–3.46	–4.14	–3.93	–3.51
M_{FeB3}	–3.39	–4.11	–3.90	–3.54
M_{FeB4}	–3.43	–3.58	–3.98	–3.43
M_{FeB5}	–3.41	–4.13	–3.95	–3.46
M_{FeB6}	–3.37	–4.11	–3.94	–3.48
ΔE	966	105	0	327
<i>P2/c</i> symmetry				
M_{total}	4.00(–)	4.00	4.00	2.00
M_{FeA1}	3.48	4.08	4.09	4.08
M_{FeA2}	3.46	4.06	4.08	4.07
M_{FeB1}	–3.53	–3.57	3.83	–3.50
M_{FeB2}	–3.51	–3.56	3.83	–3.51
M_{FeB3}	–3.67	–3.56	3.97	–3.45
M_{FeB4}	–3.39	–3.55	3.89	–3.46
M_{FeB5}	–3.40	–4.01	3.84	–3.47
M_{FeB6}	–3.57	–4.05	3.87	–3.50
ΔE	841	108	0	337

loss of band formation energy by far outweighs the gain in localization energy. So, there is a strong competition between localization and band formation/hybridization energies, and in the simple Verwey scenario the loss in band formation energy, due to localization of one additional electron on the B2 octahedral sites, is three times larger than the gain in localization energy. This balance could possibly be reversed by increasing the nearest-neighbor Fe-(B2-type) O bond length, which could perhaps be realized in a very distorted structure, although it is not the case for the orthorhombic structures studied here. The expectation is that substantially increased Fe-(B2-type) O bond length would lead to an increase in the localization energy of all six *d* electrons of B2-Fe (with 2+ valency), and a reduction of their hybridization, thus establishing the Verwey phase as the lowest-energy solution. However, one should keep in mind that we refer to nominal valencies, and therefore find that already Fe³⁺ contains more than five *d* electrons (Table III). All in all, Fe₃O₄ turns out to have mostly intermediate valencies.

Inspecting in detail the other numbers of Table I, where the results for cubic structure are summarized, one can see that because these systems are either insulating or half me-

TABLE III. Listed are the numbers of spin-up and spin-down valence electrons on the respective Fe-atom types for the LSD (two types only) and three different SIC-LSD calculations for the cubic structure.

Scenario	Fe _A [↑]	Fe _A [↓]	Fe _{B1} [↑]	Fe _{B1} [↓]	Fe _{B2} [↑]	Fe _{B2} [↓]
LSD	5.06	1.67	2.15	5.71	2.15	5.71
SIC(1)	5.34	1.34	2.24	5.81	1.82	5.90
SIC(2)	5.35	1.33	1.97	5.87	1.97	5.87
SIC(3)	5.36	1.35	2.26	5.73	2.26	5.73

tallic their total magnetic moments are integer. The corresponding total spin magnetic moments for LSD, scenario SIC(1), and scenario SIC(2) are equal to $4.0\mu_B$ per formula unit, while for the third scenario the total spin moment is $2.0\mu_B$ per formula unit. The latter value results from the fact that for divalent ions, one additional *d* electron becomes localized. The type-resolved octahedral sites spin magnetic moments are substantially larger for the trivalent ions than for the divalent ions in all the SIC-LSD calculations. The spin magnetic moments of the tetrahedral Fe's are of similar magnitude but opposite sign to the trivalent octahedral ions. As there are twice as many octahedral sites as tetrahedral ones, the total spin magnetic moment of magnetite in all the different scenarios is mostly due to the octahedral sites. The SIC-LSD spin magnetic moments of the oxygens are of the order of $(0.02-0.30)\mu_B$, depending on the scenario, while the spin magnetic moments on the empty spheres are still two orders of magnitude smaller. It is interesting that for the scenario with all octahedral ions in divalent configuration all oxygen moments are oppositely polarized to the octahedral Fe moments and are of the order of $0.2-0.3\mu_B$. This of course is reflected in the much smaller total spin moment of this scenario. For the first and second scenarios the O moments are smaller, between $0.04\mu_B$ and $0.17\mu_B$, and polarized parallel to the octahedral Fe ions. The oxygen moments calculated within LSD are of the order of $0.1\mu_B$ and aligned antiparallel to the octahedral Fe spin magnetic moments.

Turning to Table II (orthorhombic structure), one can see similar behavior to that of Table I (cubic structure). Except for the LSD, the respective energy differences for different scenarios are slightly smaller, but otherwise comparable to those for the cubic structure. Regarding the type of solution, metallic or otherwise, again the scenario SIC(1) is insulating, for both orthorhombic structures, but the second (all trivalent) scenario for *Pmc2₁* symmetry and LSD for the *P2/c* symmetry are not 100% spin polarized, as reflected by their respective total spin magnetic moments. Most importantly, however, for the refined atom positions, as reflected by the structure with *P2/c* symmetry,⁷ the all trivalent scenario is half metallic. Also, for the LSD solution in this structure we find only a minute deviation from 100% spin polarization with the DOS at the Fermi level of about 0.24 states per formula unit and the total spin magnetic moment of almost $4.00\mu_B$ (with the accuracy better than 0.5%). Compared to the other orthorhombic structure^{5,6} it appears that the refined atom positions are crucial for the half-metallic solution in the second scenario. Regarding the type-resolved spin magnetic

TABLE IV. Listed are the numbers of spin-up and -down valence electrons on the respective Fe-atom types for the LSD (two types only) and three different SIC-LSD calculations for the orthorhombic structures.

	LSD	SIC(1)	SIC(2)	SIC(3)
<i>Pmc2₁</i> symmetry				
Fe _{A1} [↑]	5.41	5.73	5.74	5.75
Fe _{A1} [↓]	2.02	1.60	1.60	1.60
Fe _{A2} [↑]	5.35	5.71	5.71	5.73
Fe _{A2} [↓]	2.03	1.58	1.58	1.58
Fe _{A3} [↑]	5.33	5.71	5.72	5.74
Fe _{A3} [↓]	2.03	1.57	1.56	1.57
Fe _{A4} [↑]	5.28	5.64	5.65	5.66
Fe _{A4} [↓]	1.94	1.49	1.49	1.50
Fe _{B1} [↑]	2.28	2.29	2.04	2.29
Fe _{B1} [↓]	5.68	5.87	5.92	5.79
Fe _{B2} [↑]	2.21	1.80	1.97	2.26
Fe _{B2} [↓]	5.67	5.94	5.90	5.77
Fe _{B3} [↑]	2.19	1.77	1.95	2.20
Fe _{B3} [↓]	5.58	5.88	5.85	5.74
Fe _{B4} [↑]	2.20	2.24	1.92	2.28
Fe _{B4} [↓]	5.63	5.82	5.90	5.71
Fe _{B5} [↑]	2.19	1.76	1.91	2.24
Fe _{B5} [↓]	5.60	5.89	5.86	5.70
Fe _{B6} [↑]	2.22	1.79	1.93	2.24
Fe _{B6} [↓]	5.59	5.90	5.87	5.72
<i>P2/c</i> symmetry				
Fe _{A1} [↑]	5.05	5.32	5.33	5.34
Fe _{A1} [↓]	1.57	1.24	1.24	1.26
Fe _{A2} [↑]	5.04	5.31	5.32	5.33
Fe _{A2} [↓]	1.58	1.25	1.24	1.26
Fe _{B1} [↑]	2.01	2.08	1.86	2.09
Fe _{B1} [↓]	5.54	5.65	5.69	5.59
Fe _{B2} [↑]	2.04	2.09	1.88	2.10
Fe _{B2} [↓]	5.55	5.65	5.71	5.61
Fe _{B3} [↑]	1.88	2.04	1.72	2.07
Fe _{B3} [↓]	5.55	5.60	5.69	5.52
Fe _{B4} [↑]	1.92	1.95	1.67	1.97
Fe _{B4} [↓]	5.31	5.50	5.56	5.43
Fe _{B5} [↑]	1.93	1.57	1.72	1.97
Fe _{B5} [↓]	5.33	5.58	5.56	5.44
Fe _{B6} [↑]	1.95	1.65	1.79	2.05
Fe _{B6} [↓]	5.52	5.70	5.66	5.55

moments, again we see that the trivalent tetrahedral and octahedral sites give rise to comparable values, with substantially smaller moments of the divalent Fe octahedral sites. Also, the oxygen spin moments are similar to those of the cubic structure.

The spin resolved charges for various Fe atoms for all scenarios and structures are given in Tables III and IV. The first thing to note is that except for the LSD scenario the electron charges of both spin components of the tetrahedral Fe's do not differ too much among various scenarios. The

situation is different for the octahedral sites. Especially, in the Verwey charge ordered scenario the different octahedral ions show similar numbers in one spin component, but differ by about 0.42 electron in the other spin component of the cubic structure, which is due to localization of the sixth *d* electron. So, while in the ionic picture the valency of the two octahedral sites (*B1* and *B2*) differs by 1, in terms of the charge disproportionation they are only 0.32 electron different. The situation is similar for the orthorhombic structures. For the structure with the *Pmc2₁* symmetry the *B1* and *B4* sites are divalent, while *B2*, *B3*, *B5*, and *B6* sites are trivalent. In the other orthorhombic *P2/c* structure, the sites *B1* to *B4* are divalent, while *B5* and *B6* sites are trivalent. Again, the charge of spin-down components of all the octahedral sites is of the order of 5.8–5.9 electron, the spin-up charges of the divalent sites are about 2.2–2.3 electron, while for the trivalent sites they are of the order of 1.8 electron for the *Pmc2₁* symmetry. For the *P2/c* symmetry the spin-down charges of the octahedral sites fall between 5.5 and 5.7 electron, while the spin-down charges are of the order of 2.0 and 1.6–1.7 electron for the divalent and trivalent octahedral ions, respectively. Consequently, the total charge disproportionation between the divalent and trivalent sites is up to 0.5 and 0.6 electron, respectively, for the *Pmc2₁* and *P2/c* symmetries. There is a spread in charges over the octahedral sites of the orthorhombic structures due to the reduced symmetry of these Fe sites. In the orthorhombic structure we also see charge disproportionation in the other three scenarios, namely, LSD, scenario SIC(2), and SIC(3)—this of course does not occur in the cubic phase. It is important to note that for the ground-state configuration of all trivalent Fe's we find charge disproportionations of 0.2 and 0.36 electron for the *Pmc2₁* and *P2/c* symmetries, respectively. These calculated charge disproportionations are in better agreement with the recent experimental study by Wright *et al.*⁷ than the ones of the Verwey charge ordered state.

V. CONCLUSIONS

In summary, in the present application of the first-principles SIC-LSD method to magnetite we have studied three different arrangements of Fe's on the octahedral sites, namely, the simple Verwey order, the case where, similar to the tetrahedral sites, all the octahedral sites have been occupied by Fe³⁺, and finally the scenario with all the octahedral sites occupied by the Fe²⁺ ions. For all these scenarios the tetrahedral sites have been occupied only by Fe³⁺. Our total-energy calculations, both for the cubic and orthorhombic structures, have shown that the second scenario, with all interstitial sites occupied by Fe³⁺, is the ground-state solution, followed by the case of the Verwey charge order. In the latter case, we have calculated magnetite to be insulating with a gap of about 0.35 eV (~0.1 eV in the orthorhombic phase), while the Fe³⁺ scenario, depending on structure, has given rise to half-metallic or metallic (though still with high spin polarization) state. The insulating state for the Verwey scenario indicates that in the SIC-LSD description the O 2*p* bands are filled, as would be the case for the ionic model.

However, no ionic charge distribution is obtained as substantial Fe and O bonding and hybridization still occur. Localizing one less Fe *d* electron (second scenario) results in the disappearance of the insulating state and emergence of the half-metallic state, which is a nontrivial result, not predicted by the ionic model.

The ground-state scenario of all trivalent Fe's gives a charge disproportionation which is approximately half of what is found in the Verwey charge ordered state in the orthorhombic structure. The values of the ground-state scenario are in line with the recent experiments.^{7,11,12} The charge disproportionation in the ground state is similar to the one obtained from the LSD which would indicate that these charge disproportionations are not of an electronic origin but are determined by the structure. Namely, the inequivalent Fe positions give rise to different charge distributions, while the nominal Fe valency remains unaltered.

Obviously we have managed to study only the three simplest charge ordering scenarios, and within these restrictions our results indicate the energetically unfavorable character of Fe²⁺. We also find the same ground-state configuration of all trivalent Fe's in both the cubic structure and the distorted orthorhombic structures. The calculations indicate no minority-spin electron localization in the distorted structure, only a marginal decrease, in this structure, with respect to the cubic one, of 5% or so, in the energy difference between the ground state and the charge ordered one. This implies that a simple charge ordered state as described by scenario 1 [SIC(1)] is not realized below the Verwey temperature.

Our study has shown that the SIC-LSD is capable to study any kind of static charge order, although realization of more complicated charge arrangements, which might be of relevance to future studies, may be limited by memory and CPU of present computers. Given these limitations that we only studied a simple Verwey charge ordered state, we have concluded that the charge disproportionation below the Verwey temperature is structural in origin and all Fe ions occur in a trivalent state. This does not exclude the possibility that Fe₃O₄ below the Verwey temperature is described by a much more complicated charge ordered state.

ACKNOWLEDGMENTS

We thank Dr. P. G. Radaelli for providing atom positions of the orthorhombic structure with *P2/c* symmetry, Professor Victor Antonov for useful communication, and Professor P. H. Dederichs for valuable discussions. This work was partially funded by the Training and Mobility Network on "Electronic Structure Calculation of Materials Properties and Processes for Industry and Basic Sciences" (Contract No. FMRX-CT98-0178) and the Research Training Network "Psi-k f-electron" (Contract No. HPRN-CT-2002-00295). This work was partially sponsored by the Division of Materials Sciences and Engineering, Office of Basic Energy Sciences, U.S. Department of Energy, under Contract No. DE-AC05-00OR227725. The computational work reported here was performed at the Center for Computational Sciences (CCS) at ORNL and at NERSC at LBNL.

¹Friedrich Walz, J. Phys.: Condens. Matter **14**, R285 (2002).

²E.J.W. Verwey and P.W. Haayman, Physica (Utrecht) **8**, 979 (1941); E.J.W. Verwey, P.W. Haayman, and F.C. Romeijn, J. Chem. Phys. **15**, 181 (1947).

³S.K. Park, T. Ishikawa, and Y. Tokura, Phys. Rev. B **58**, 3717 (1998).

⁴M. Imada, A. Fujimore, and Y. Tokura, Rev. Mod. Phys. **70**, 1039 (1998).

⁵M. Iizumi, T.F. Koetzle, G. Shirane, S. Chikazumi, M. Matsui, and S. Todo, Acta Crystallogr., Sect. B: Struct. Crystallogr. Cryst. Chem. B **38**, 2121 (1982).

⁶J.M. Zuo, J.C.H. Spence, and W. Petuskey, Phys. Rev. B **42**, 8451 (1990).

⁷J.P. Wright, J.P. Attfield, and P.G. Radaelli, Phys. Rev. Lett. **87**, 266401 (2001).

⁸F.J. Berry, S. Skinner, and M.F. Thomas, J. Phys.: Condens. Matter **10**, 215 (1998).

⁹H.P. Rooksby and B.T.M. Willis, Acta Crystallogr. **6**, 565 (1953).

¹⁰P.W. Anderson, Phys. Rev. **102**, 1008 (1956).

¹¹J. García, G. Subías, M.G. Proietti, H. Renevier, Y. Joly, J.L.

Hodeau, J. Blasco, M.C. Sánchez, and J.F. Béar, Phys. Rev. Lett. **85**, 578 (2000).

¹²J. García, G. Subías, M.G. Proietti, J. Blasco, H. Renevier, J.L. Hodeau, and Y. Joly, Phys. Rev. B **63**, 054110 (2001).

¹³P. Strange, A. Svane, W.M. Temmerman, Z. Szotek, and H. Winter, Nature (London) **399**, 756 (1999).

¹⁴Z. Zhang and S. Satpathy, Phys. Rev. B **44**, 13 319 (1991).

¹⁵V.I. Anisimov, I.S. Elfimov, N. Hamada, and K. Terakura, Phys. Rev. B **54**, 4387 (1996).

¹⁶V.N. Antonov, B.N. Harmon, V.P. Antropov, A.Ya. Perlov, and A.N. Yaresko, Phys. Rev. B **64**, 134410 (2001).

¹⁷J.P. Perdew and A. Zunger, Phys. Rev. B **23**, 5048 (1981).

¹⁸W.M. Temmerman, A. Svane, Z. Szotek, and H. Winter, in *Electronic Density Functional Theory: Recent Progress and New Directions*, edited by J.F. Dobson, G. Vignale, and M.P. Das (Plenum Press, New York, 1998).

¹⁹O.K. Andersen, Phys. Rev. B **12**, 3060 (1975).

²⁰O.K. Andersen and O. Jepsen, Phys. Rev. Lett. **53**, 2571 (1984).

²¹W.R.L. Lambrecht and O.K. Andersen, Phys. Rev. B **34**, 2439 (1986).